Ocean Engineering 170 (2018) 100–110

Contents lists available at ScienceDirect

Ocean Engineering

journal homepage: www.elsevier.com/locate/oceaneng

Novel DVS guidance and path-following control for underactuated ships in presence of multiple static and moving obstacles

Guoqing Zhang[a,b,c], Yingjie Deng[a], Weidong Zhang[c,*], Chenfeng Huang[a]

[a] Navigation College, Dalian Maritime University, Dalian, 116026, Liaoning, PR China
[b] Collaborative Innovation Center for Transport Studies, Dalian Maritime University, Dalian, 116026, Liaoning, PR China
[c] Department of Automation, Shanghai Jiao Tong University, Shanghai, 200240, PR China

ARTICLE INFO

Keywords:
Underactuated ships
Guidance principle
Path-following
Obstacles avoidance
Finite-time control

ABSTRACT

This note focuses on the waypoints-based path-following problem of underactuated ships, where the reference path is surrounded by multiple static and moving obstacles. By virtue of the improved dynamical virtual ship (DVS) principle, a novel guidance law with multi-obstacles avoidance is proposed to generate the real-time attitude reference. In this approach, the manoeuvering tasks are specified as three priority levels: the static obstacle avoidance, the moving obstacle avoidance and the path-following mission. And the detailed design abides the International Regulations for Preventing Collisions at Sea (COLREGs) to ensure the sailing safety, especially for moving obstacles or other vessels. Furthermore, a robust neural algorithm is developed by using the neural networks (NNs) approximation and the robust neural damping technique. The system gain uncertainty of actuators is tackled and less information about the hydrodynamic structure, the actuator model and the external disturbances are required. Considerable efforts are made to obtain the semi-global practical finite-time bounded (SGPFB) stability. The proposed scheme is with advantages of concise structure and improved autonomy. Finally, two experiments are employed to verify the effectiveness of the proposed strategy.

1. Introduction

Over the last few years, control of underactuated ships has attracted attention from the community of ocean engineering, e.g. missions of the path-following (Zhang et al., 2017b; Lin et al., 2018), the trajectory-tracking (Park, 2017), the formation control (Shojaei, 2016), etc. Especially, the path-following control is a meaningful issue for its superiorities in aspects of saving energy and improving the vehicle's autonomy (Kozynchenko and Kozynchenko, 2018; Campbell et al., 2012). Though, to the author's best knowledge, few studies have concerned on the integration of path-following control with the mechanism of obstacles avoidance in the existing literature (Fossen and Pettersen, 2014). In the marine practice, the obstacles and collision avoidance manoeuvering is inevitable when steering a ship in the predetermined route, e.g. the fishing or reef area. Therefore, it is imperative to develop a novel path-following scheme with the obstacles avoidance mechanism, which is significant for enhancing the security and autonomy of marine vehicles (Zhang and Zhang, 2016).

In the existing literature, the problem of static obstacles avoidance is usually addressed by the path planning algorithm (Tae Hwan Lee and Myung, 2011; Tam et al., 2009), e.g. chains of islands and the large-scale submerged rock. However, the sailing situation is polytropic due to the tidal variation and moving obstacles surrounding the reference path. The obstacles avoidance manoeuvering should be carried out in real-time from the guidance level. The line-of-sight (LOS) algorithm is a common guidance principle in the scene of straight-line path-following mission (Fossen, 2011; Caharija et al., 2014). It first sets the desired heading angle ψ_d based on the ship's bearing to the upcoming waypoint. Then the control objective $\psi \to \psi_d$ is implemented by the course keeping controller. Around more practical missions, the ships' path-following and obstacle avoidance are achieved in (Moe and Pettersen, 2016) by incorporating the set-based theory into the LOS guidance. And that is subject to the related collision prevention regulation (i.e. COLREGs). In (Naeem et al., 2012), a manual biasing scheme is further developed to enhance the COLREGs-compliant capability. Nevertheless, the automatic manoeuvering is only achieved by altering the desired yaw angle, without regulating the surge speed. The above mentioned researches only tackle the situation of encountering single obstacle. Actually, the obstacles avoidance issue of marine ships could be addressed by employing the result in field of mobile robot, e.g. the method of potential fields (Khatib, 1986; Liu and Bucknall, 2015), the behavior-based reactive obstacles avoidance approach (Rodríguez-Seda et al.,

* Corresponding author. Department of Automation, Shanghai Jiao Tong University, Shanghai, 200240, PR China.
E-mail addresses: zgq_dlmu@163.com (G. Zhang), wdzhang@sjtu.edu.cn (W. Zhang).

https://doi.org/10.1016/j.oceaneng.2018.10.009
Received 2 February 2018; Received in revised form 3 October 2018; Accepted 5 October 2018
Available online 17 October 2018

2014). In (Zereik et al., 2015), the navigation guidance and control system is designed by utilizing a priority task approach, which allows to separate the different tasks required to the robot and to incorporate them into the desired full autonomy. And the ODEs (ordinary differential equations) based method for real-time obstacle avoidance proposed in (Soltan et al., 2011) solved the practical trajectory planning issue for the unmanned surface vehicle. The ODEs are employed to define transitional trajectories that can avoid the moving obstacles and reach to the final desired target using a robust tracking controller. Although, there still exist some constraints in the marine practice that could restrict the implementation of the aforementioned results. E.g. the ship is with the characteristics of great inertia and long time delay (Zhang and Zhang, 2014; Zhang et al., 2017a), and the practical reference path is defined by the waypoints in the electronic chart (Fossen, 2011).

As for the path-following control, a variety of theoretical studies have been developed by resorting to the novel analytic tools and strategies, e.g. the time-varying feedback method (Do and Pan, 2006; Li et al., 2008; Liu et al., 2016)and the discontinuous ones (Godhavn et al., 1998; Ghommam et al., 2010). In (Godhavn et al., 1998), a continuous time invariant control law was developed for underactuated ships. However, the orientation was not stabilized to avoid undesired whirling around in the vicinity of the reference path. Furthermore, Li et al. (2008) developed a adaptive controller for the point-to-point navigation. And the conclusion, about the passive boundedness of the sway motion, was presented and proofed by virtue of the Lyapunov theory. To tackle more practical issue, one employed the NNs (Li et al., 2015, 2017; Zhao et al., 2014) to approximate the system structure and parameter uncertainty in the authors' previous work (Zhang and Zhang, 2014). The actual control law is with the burdensome merit and easy to be implemented in practice. In (Zhang and Zhang, 2015, 2016), the constraint of actuators' gain uncertainty is released by utilizing the DSC(dynamic surface control) and robust neural damping techniques. In addition, the saturation effect of actuators could be compensated for the dynamical attitudes allocation of DVS. Actually, the path-following problem considered in the afore literature is solved by the asymptotic stability analysis, which means that the marine ship converges to the reference equilibrium with the infinite settling time. It is well known that the finite-time stabilization of dynamical plant is with a better closed-loop performance in aspects of disturbance attenuation and fast convergence to the origin (Zou et al., 2011; Wang et al., 2016). In (Wang et al., 2016), the robust finite-time tracking design is ingenious and the possible chattering problem is avoided.

Motivated by the above observations, this note focus on the guidance and control design for underactuated ship in presence of multiple static and moving obstacles, where the obstacles' dimension is sizable to the real ship. That could ensure that the related information around obstacles is measurable. A novel DVS-based path-following control scheme is developed to facilitate the full autonomy of underactuated ships. In the scheme, the control inputs of interest are two steerable variables: the shaft speed n and the rudder angle δ. The main contribution of this note can be summarized as follows:

(1) A novel DVS-based obstacles avoidance guidance, with a priority selecting strategy, is developed for underactuated ships. Under the principle, the real ship could auto-navigate along with the waypoints-based reference path, considering avoidance of the multi-static and multi-moving obstacles. In addition, the principle complies with the COLREGs and could smoothly switch between the path-following and obstacles avoidance mode.
(2) The robust adaptive path-following control law is derived with the finite-time convergence property, taking the shaft speed n of propeller and the rudder angle δ as the control input. In this algorithm, no information on the system inertia and the external disturbance is required. Only two gain-related adaptive parameters are updated online. That leads to the concise form of the controller, and could facilitate its application in practice.

2. Problem formulation

2.1. Ship dynamics

In this note, the plant of interested is the marine surface ship with a single rudder and propeller, i.e. the underactuated ship. According to the Newtonian or Lagrangian mechanics (Fossen, 2011; Zhang and Zhang, 2016), the mathematical model of an underactuated ship moving in horizontal plane is described as Eqs. (1) and (2).

$$\begin{cases} \dot{x} = u\cos(\psi) - v\sin(\psi), \\ \dot{y} = u\sin(\psi) + v\cos(\psi), \\ \dot{\psi} = r \end{cases} \tag{1}$$

$$\begin{cases} \dot{u} = f_u(\boldsymbol{\nu}) + \frac{T_u}{m_u}|n|n + d_{wu} \\ \dot{v} = f_v(\boldsymbol{\nu}) + d_{wv} \\ \dot{r} = f_r(\boldsymbol{\nu}) + \frac{F_r}{m_r}\delta + d_{wr} \end{cases} \tag{2}$$

with the nonlinear inertia and damping terms:

$$\begin{aligned} f_u(\boldsymbol{\nu}) &= \frac{m_v}{m_u}vr - \frac{d_u}{m_u}u - \frac{d_{u2}}{m_u}|u|u - \frac{d_{u3}}{m_u}u^3, \\ f_v(\boldsymbol{\nu}) &= -\frac{m_u}{m_v}ur - \frac{d_v}{m_v}v - \frac{d_{v2}}{m_v}|v|v - \frac{d_{v3}}{m_v}v^3, \\ f_r(\boldsymbol{\nu}) &= \frac{(m_u - m_v)}{m_r}uv - \frac{d_r}{m_r}r - \frac{d_{r2}}{m_r}|r|r - \frac{d_{r3}}{m_r}r^3 \end{aligned} \tag{3}$$

where $[x, y, \psi]^T \in \Re^3$ are the surge, sway displacement and yaw angle in the earth fixed coordinate system, and $\boldsymbol{\nu} = [u, v, r]^T \in \Re^3$ denotes the surge, sway, and yaw velocities. In this model, n, δ are selected as the control inputs: the shaft speed and the rudder angle instead of the propulsion force and torque that are less measurable in the practical engineering (Yu et al., 2017). Furthermore, T_u, F_r are derived to describe the corresponding gain uncertainty due to the actuated servo systems. That could increase the difficulty to the control design. As for the model parameters, m_u, m_v, m_r are additional mass in three degree of freedom. d_u, d_v, d_r, d_{u2}, d_{v2}, d_{r2}, d_{u3}, d_{v3}, d_{r3} are employed to describe the hydrodynamic damping terms. Actually, for the control design, the nonlinear functions $f_u(\boldsymbol{\nu})$, $f_v(\boldsymbol{\nu})$, $f_r(\boldsymbol{\nu})$ are unknown in structure with uncertain parameters. d_{wu}, d_{wv}, d_{wr} describe the unmodeled dynamics and the immeasurable external disturbance forces and moment caused by waves, wind, and ocean current.

Remark 1. *The nonlinear mathematical model (1) and (2) has been employed in* (Zhang and Zhang, 2015), *which is only for the control design. In marine practice, the ship is underactuated as there is only two independent controls, i.e. n and δ. And the rudder, which mainly affects the yaw motion, also influences the surge and sway dynamics. E.g., according to the physical reasoning theory in the literature* (Zhang et al., 2015), *the rudder's actuating forces (or moments) can be formulated as* $(1 - t_R)F_N\sin\delta$, $(1 + a_H)F_N\cos\delta$, $(x_R + a_H x_H)F_N\cos\delta$ *for the surge, sway and yaw motions, respectively, where* t_R, a_H, x_R, x_H *are the interference coefficients and the dimension parameters. Eq.(4) presents briefly the generation mechanism of the pressure force* F_N *perpendicularly acting on the rudder blade. The effective attack angle* α_R *is a small value, and the approximation relationship* $\sin\alpha_R \approx \alpha_R \approx \delta$ *holds for* $\delta \in [-0.5236\text{rad}, 0.5236\text{rad}]$. *Considering that the impact forces* $(1 - t_R)F_N\sin\delta$ *and* $(1 + a_H)F_N\cos\delta$ *are slight, they are dealt with as the disturbances in Eq.(2). Hence, the system model is reasonable and is the basis of the following design.*

$$F_N = -\frac{6.13\Lambda}{\Lambda + 2.25}\cdot\frac{A_R}{L^2}(u_R^2 + v_R^2)\sin\alpha_R \tag{4}$$

In addition, since the actuators' energy gain is certainly positive and finite, there exist unknown constants T_{u0}, $\bar{T}_u$, F_{r0}, $\bar{F}_r$ such that $0 < T_{u0} \le T_u \le \bar{T}_u$, $0 < F_{r0} \le F_r \le \bar{F}_r$.

Assumption 1. There exist unknown positive constants $\bar{d}_{wu}$, $\bar{d}_{wv}$, $\bar{d}_{wr}$,

such that the disturbance terms satisfy $d_{wu} \le \bar{d}_{wu}$, $d_{wv} \le \bar{d}_{wv}$, $d_{wr} \le \bar{d}_{wr}$.

Assumption 2. *Based on the systematic analysis in* (Li et al., 2008; Do, 2010), *the sway motion of underactuated ships is passive-bounded stable. It means that the sway velocity v is bounded as the surge and yaw motions are uniform ultimate bounded.*

Assumption 3. *Considering that the onboard detective facilities are with the finite operating distance,* e.g. *the laser radar or the visual sensor* (Rodríguez-Seda et al., 2014), *it is assumed that the real ship could measure the dynamics of obstacles within the detectable space (i.e. a round region with the radius R_m), including their center coordinates, heading angle and velocity.*

The objective of this note includes two points: (1) to develop a DVS-based guidance approach which is able to provide the reference planning and the multiple obstacles avoidance guidance. (2) to design a practical finite-time control law to stabilize the error dynamic system between the real ship and the DVS.

2.2. Some useful lemmas

Some useful lemmas, which facilitate the control design, are introduced as follows.

Lemma 1. (Zou et al., 2011) *Consider the system $\dot{\mathbf{x}} = f(\mathbf{x})$, $\mathbf{x} \in \Omega \subset \Re^n$, $f(0) = 0$, if there exists a continuous Lyapunov function $V(\mathbf{x}) \ge 0$, and scalars $c_1 > 0$, $\varsigma > 0$ such that*

$$\dot{V}(\boldsymbol{x}) \le -c_1 V^p(\boldsymbol{x}) + \varsigma, \quad p \in (0,1) \tag{5}$$

Then, the nonlinear system $\dot{\mathbf{x}} = f(\mathbf{x})$ is SGPFB, and the trajectory of the closed-loop system converges to a compact set containing the origin in a finite time T, i.e. $\lim_{t \to T} \mathbf{x} \in \left\{ \mathbf{x} \,\middle|\, V^p(\mathbf{x}) \le \frac{\varsigma}{(1-q)c_1} \right\}$. The settling time T is given as Eq. (6), *$0 < q < 1$ is a scalar.*

$$T = \frac{1}{(1-p)qc_1}\left[V^{1-p}(\boldsymbol{x}(0)) - \left(\frac{\varsigma}{(1-q)c_1} \right)^{(1-p)/p} \right] \tag{6}$$

Lemma 2. *For $x \in \Re$ and $0 < p = p_1/p_2 < 1, 0 < q < 1$, p_1, p_2 are positive odd integers, the following inequality (7) holds, a is a constant.*

$$-x(x+a)^p \le -\frac{1-q}{1+p}x^{1+p} + \frac{\ell}{1+p},$$
$$\ell = a^{1+p} + \left[\frac{a}{1-(1-q)^{\frac{1}{1+p}}} \right] + \left[\frac{a(1-q)^{\frac{1}{1+p}}}{1-(1-q)^{\frac{1}{1+p}}} \right]^{\frac{1}{1+p}} \tag{7}$$

Proof. See Appendix A.

Lemma 3. *For variables $a, b \in \Re$, and $p > 0$ has been defined in Lemma 2, one has*

$$ab < \frac{a^{1+p}}{1+p} + \frac{pb^{1+\frac{1}{p}}}{1+p} \le a^{1+p} + b^{1+\frac{1}{p}} \tag{8}$$

Lemma 4. (Huang et al., 2016) *For variables $x_i \in \Re$, $i = 1,2, \cdots, n$, and $0 < p \le 1$ defined in Lemma 2, then*

$$\left(\sum_{i=1}^{n} |x_i| \right)^p \le \sum_{i=1}^{n} |x_i|^p \le n^{1-p} \left(\sum_{i=1}^{n} |x_i| \right)^p \tag{9}$$

Lemma 5. (Chen et al., 2009; Li et al., 2010) *For any smooth function $f(\mathbf{x})$, $f(0) = 0$ defined in a compact set $\Omega_x \subset \Re^m$, applying the principle of continuous function separation, a RBF NNs (radial basis function neural networks) described as* Eq. (10) is able to approximate it with any precision.

$$f(\boldsymbol{x}) = \boldsymbol{S}(\boldsymbol{x})\boldsymbol{A}\boldsymbol{x} + \varepsilon, \quad \forall\, \boldsymbol{x} \in \Omega_x \tag{10}$$

where $\mathbf{S}(\mathbf{x}) = [s_1(\mathbf{x}), s_2(\mathbf{x}), \cdots, s_l(\mathbf{x})]$ is the Gaussian function vector composed of the following elements (11), *l is the node number of NNs. $\boldsymbol{\mu}_i$ denotes the core of the receptive field and ξ_i is the width of the Gaussian function. In addition, $\mathbf{A} \in \Re^{l \times m}$ is the optimal weight matrix, $\varepsilon(\mathbf{x})$ is the approximating error with the unknown upper bound $\bar{\varepsilon}$.*

$$s_i(\boldsymbol{x}) = \frac{1}{\sqrt{2\pi}\xi_i} \exp\left(-\frac{(\boldsymbol{x} - \boldsymbol{\mu}_i)^{\mathrm{T}}(\boldsymbol{x} - \boldsymbol{\mu}_i)}{2\xi_i^2} \right), \; i = 1, \cdots, l \tag{11}$$

3. DVS guidance with the obstacles avoidance function

In order to improve the autonomy of underactuated ships in the complex multi-obstacles situation, the guidance strategy should possess multiple functions, e.g. the path-following and the obstacles avoidance mission. For this purpose, this part presents the improved version of DVS guidance to facilitate the intelligent navigation of marine ships. The proposed guidance law is to provide an attitude or velocity reference, which makes the reasonable connection between the real ship and the waypoints-based reference. That is, the dynamics of guidance virtual ship (GVS) is calculated logically on basis of the waypoints' information and the DVS is dynamically assigned to follow GVS. The controller in Section 4 is to control the real ship to follow DVS.

Fig. 1 gives the basic framework of the proposed guidance law. The reference path is usually set by the waypoints $W_1, W_2, \cdots, W_n$ with $W_i = (x_i, y_i)$, which guides the real ship sailing in the open sea. The GVS and the DVS are two key elements in the guidance law, satisfying the standard kinematic equation (12). Based on the coordinate information of waypoints W_{i-1}, W_i and W_{i+1}, the input orders u_g, r_g for GVS could be obtained analytically by splitting the reference path into regular straight lines and smooth arcs: $W_{i-1}P_{\mathrm{in}W_i}$, $P_{\mathrm{out}W_i}$ and arc_{W_i}. More details are referred in the author's previous work (Zhang and Zhang, 2015).

$$\begin{cases} \dot{x}_i = u_i \cos(\psi_i) \\ \dot{y}_i = u_i \sin(\psi_i), \quad i = g, d \\ \dot{\psi}_i = r_i \end{cases} \tag{12}$$

As shown in Fig. 1, the DVS is assigned with the attitude or velocity reference based on the interactive situation between the real ship and GVS, as the direct tracking objective of the real ship. Different from (Zhang and Zhang, 2015), one develops a novel assigned strategy in this section to cope with the practical sailing situations, e.g. no obstacles and encountering multi-obstacles. Those correspond to the two guidance modes (i.e. path-following and obstacles avoidance), which rest with the immediate coordinates of the real ship relative to the obstacles. Actually, when the real ship sails with the autopilot, the control law would actuate the real ship to the small vicinity region of the DVS and the related design procedures would be illustrated in Section 4.

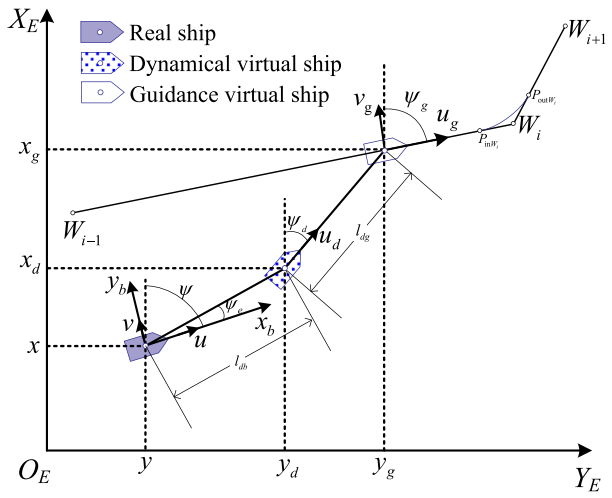

Fig. 1. Basic framework of the improved DVS guidance.

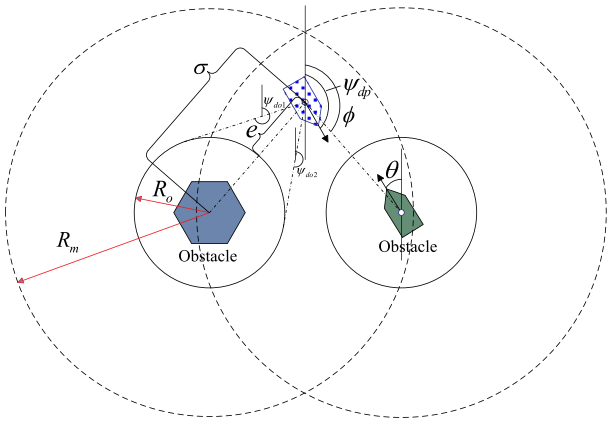

Fig. 2. Parameters interpretation for the improved DVS guidance.

Therefore, it is assumed that the DVS in this part is with the same capability of obstacles detecting and that is reasonable in the marine practice. To quantitatively describe the principle, one defines the detectable space and the anti-collision space by using the R_m, R_o shown in Fig. 2. From the Assumption 3, the maximum of R_m rests with the measurability of the onboard detective facilities and is constant for different obstacles. Whereas, R_o varies with the characteristic of obstacles, e.g. the dynamics, the size, etc. Therefore, the detectable and anti-collision spaces are marked upon the obstacles in this principle, see Fig. 2. In the following, the assigned strategies are detailed for the path-following mode and the obstacles avoidance one.

Case 1. Path-following mode. In Fig. 2, if the DVS is located out of the detectable spaces of obstacles, i.e. $\sigma > R_m$, the path-following mode is activated. Under this case, the DVS is always assigned as $\psi_d = \psi_{dp}$, $u_d = u_{dp}$. And the yawing angle ψ_{dp} can be calculated by Eq. (13), i.e. the true azimuth angle of GVS. In Eq. (13), sgn is the sign function. For a given scalar a, sgn(a) = 1 when $a \geq 0$, and sgn(a) = −1 for $a < 0$. The speed u_{dp} is obtained by Eq. (14).

$$\psi_{dp} = 0.5\,\mathrm{sgn}(y_g - y_d)[1 - \mathrm{sgn}(x_g - x_d)]\cdot\pi + \arctan\left(\frac{y_g - y_d}{x_g - x_d}\right) \tag{13}$$

$$u_{dp} = [k_d l_{dg} + u_g \cos(\psi_g - \psi_d)]\cdot\frac{l_{dbset} - l_{db}}{l_{dbset}} \tag{14}$$

where k_d is a positive design parameter, l_{dg}, l_{db} represents the following distances of DVS, GVS and the real ship. Note that l_{dbset} is a threshold parameter to prevent the real ship's propulsion constraints. For example, the real ship may deviate largely from the DVS due to the obstacles avoidance manoeuvering or other causes. In general, the large following error requires to be compensated by the large thruster force. Using Eq. (14), when $l_{db} = l_{dbset}$, $u_{dp} = 0$, DVS desires to be slowed down to weaken the saturation effect. Thus, the limitation of actuators could be tackled through tuning the parameter l_{dbset}.

In the further analysis, one selects a Lyapunov-like function $V_{dg} = 0.5 l_{dg}^2$ to analysis the DVS's convergence to GVS, $l_{dg} = \sqrt{(x_g - x_d)^2 + (y_g - y_d)^2}$ has been defined in Fig. 1. The corresponding derivative is derived as Eq. (15) along with Eq. (12). Furthermore, if the real ship is stabilized to DVS, i.e. $l_{db} = 0$, it can be obtained as $\dot{V}_{dg} = -2k_d V_{dg}$ by substituting u_d into (15). Thus, it is concluded that the design of (13), (14) could guarantee the exponential convergence of DVS to the attitudes of GVS.

$$\begin{aligned}\dot{V}_{dg} &= (x_d - x_g)(\dot{x}_d - \dot{x}_g) + (y_d - y_g)(\dot{y}_d - \dot{y}_g)\\ &= l_{dg}\cos\psi_d(u_g\cos\psi_g - u_d\cos\psi_d)\\ &\quad + l_{dg}\sin\psi_d(u_g\sin\psi_g - u_d\sin\psi_d)\\ &= l_{dg}(u_g\cos(\psi_g - \psi_d) - u_d)\end{aligned} \tag{15}$$

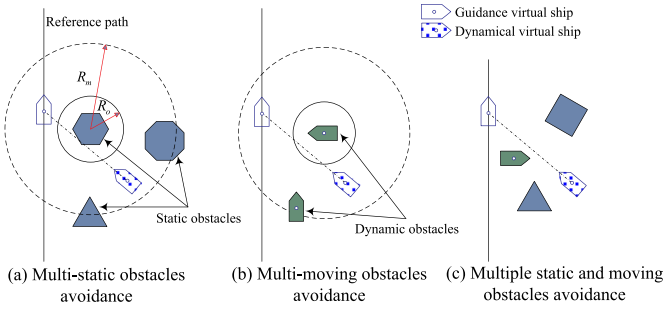

Fig. 3. Three types of obstacles avoidance situation.

Case 2. Obstacles avoidance mode. In this note, the sailing situation of multiple obstacles means that the DVS is located within the overlapped detectable space of multi-obstacles (as shown in Fig. 2), and it is a special case for the real ship to encounter the single obstacle. In this note, one defines three types of obstacles avoidance situation, see Fig. 3. A priority selecting principle is developed for the above three situations and only one obstacle is deemed as the current circumventing objective (CCO) at a time. From high to low, the three major priority levels include: the static obstacle (high), the moving obstacle (medium) and the path-following guidance (low). For each level, the avoidance sequence of obstacles is determined by the evaluation function, which would be detailed later.

Remark 2. In the proposed guidance principle, the priority selection for obstacles avoidance mode may not conform to the operator's instinct. In the marine practice, the moving obstacle, e.g. the ship under way, would keep a safe distance from the static obstacles, which is larger than the anti-collision radius R_o of the static obstacle. Following the proposed guidance law, the real ship would converge to the boundary of the corresponding anti-collision space to avoid the static obstacle. Therefore, the obstacle avoidance mechanism is also effective with respect to a moving obstacle. But conversely, there may exist collision risk between the real ship and the static obstacle. That is the basic consideration for the priority levels: the static obstacle (high), the moving obstacle (medium) and the path-following guidance (low).

(1) Situation of multi-static obstacles. In Fig. 3(a), there exist only the major priority level "the static obstacles". The priority sequence is determined according to the distance σ between the obstacle and the DVS. Meanwhile, the sailing situation of the real ship and the obstacle satisfies the collision happening condition, i.e., $\psi_{do2} \leq \psi_d \leq \psi_{do1}$ and $\sigma \leq R_m$, please refer to Fig. 2. If the collision is predictable, the static obstacles with highest priority is selected as the CCO. Then, the obstacles avoidance mode for the CCO is activated and the DVS is assigned with the avoidance speed $u_d = u_{do}$ that is a predefined constant and the heading angle $\psi_d = \psi_{do}$ as Eq. (16).

$$\psi_{do} = \phi + \lambda\left(\frac{\pi}{2} - \arctan\left(\frac{e}{\iota R_o}\right)\right),\quad \lambda = \begin{cases}-1, & \psi_{dp} > \phi\\ 1, & \psi_{dp} \leq \phi\end{cases} \tag{16}$$

where e denotes the shortest distance from the DVS to the anti-collision space of CCO, $0 < \iota < 1$ is a convergence coefficient corresponding to various convergence rates to the anti-collision space. λ denotes the counterclockwise or clockwise rotation of the CCO. The setting of λ could guarantee the shortest route of obstacles avoidance and the least voyage waste.

(2) Situation of multi-moving obstacles. As shown in Fig. 3(b), the major priority level is "the moving obstacles". For the moving obstacle, the collision condition is $\{\sigma < R_o \text{ or } R_o \leq \sigma < R_m, \dot{\sigma}_p < 0\}$, where $\dot{\sigma}_p$ represents the derivative of σ under the path-following

mode. In this situation, the priority sequence is determined by calculating the evaluation function F in the descending order. In Eq. (17), ζ is a setting weight. Then the CCO is selected as the corresponding obstacle that is with the maximum F and satisfies the collision condition. According to Assumption 3, the center coordinates x_{cco}, y_{cco} and the moving speed u_{cco} of CCO are obtainable, and the kinematics equation is with the form of Eq. (18)

$$F(e, R_m, R_o, \dot{\sigma}_p) = \begin{cases} \zeta\left(\frac{R_m - R_o - e}{R_m - R_o}\right) + (1-\zeta)\frac{-\dot{\sigma}_p}{2u_{do}}, & e > 0 \\ 2, & e \le 0 \end{cases} \tag{17}$$

$$\begin{cases} \dot{x}_{cco} = u_{cco}\cos\theta \\ \dot{y}_{cco} = u_{cco}\sin\theta \end{cases} \tag{18}$$

Once the CCO is determined, the obstacles avoidance mode is activated and the DVS is dynamically assigned with the speed $u_d = u_{do}$ and the heading angle $\psi_d = \psi_{do}$ given in Eq. (19). It should be noted that the avoidance speed u_{do} must be greater than the speed of CCO u_{cco} to ensure the effectiveness of the avoidance guidance.

$$\psi_{do} = \phi + \lambda\left(\frac{\pi}{2} - \arctan\left(\frac{e+\kappa}{\iota R_o}\right)\right) \tag{19}$$

In Eq. (19), if only one moving obstacle (e.g. a ship) is detected by the real ship, λ is chosen based on the COLREGs (Bertram, 2012; Kuwata et al., 2014). It suggests the anti-clockwise motion of the real ship for the crossing or head-on scenario ($\lambda = 1$) and either clockwise or anti-clockwise motion for the overtaking scenario ($\lambda = \pm 1$). For other cases, the selection of λ still follows Eq. (16). The variable κ is calculated by Eq. (20), which is to compensate the dynamics of the moving obstacle.

$$\kappa = \begin{cases} \frac{-b + \sqrt{b^2 - 4ac}}{2a}, & \text{for } V_o < 0 \\ \frac{-b - \sqrt{b^2 - 4ac}}{2a}, & \text{for } V_o \ge 0 \end{cases} \tag{20}$$

where $V_o = u_{cco}\cos(\pi - \phi + \theta)$ and $a = u_{do}^2 - V_o^2$, $b = -2eV_o^2$, $c = -(\iota^2 R_o^2 + e^2)V_o^2$

(3) Situation of multiple static and moving obstacles. In Fig. 3(c), there exist two major priority levels, “the static obstacles” and “the moving obstacles”. Since “the static obstacles” is with higher priority than “the moving obstacles”, one provides preference to the static obstacles to check the corresponding priority sequence. Then the sequence of moving obstacles is checked until the CCO is determined. When the obstacles avoidance mode is activated, the DVS would be assigned with the corresponding orders u_{do} and ψ_{do}, which have been detailed in parts (1) and (2). Furthermore, the path-following mode will be activated if the collision condition is relieved.

In this mode, the design of u_{do} and ψ_{do} is to guarantee that the trajectory of DVS asymptotically converge to the boundary of the CCO's anti-collision space. To illustrate their logic deduction and effectiveness, one selects the Lyapunov candidate $V_{do} = 0.5e^2$. And Eq. (21) is obvious from the geometrical relationship in Fig. 2.

$$\begin{aligned} &\sigma = \sqrt{(x_{cco} - x_d)^2 + (y_{cco} - y_d)^2}, \\ &x_{cco} - x_d = \sigma\cos\phi, \quad y_{cco} - y_d = \sigma\sin\phi \end{aligned} \tag{21}$$

The time derivative $\dot{V}_{do}$ can be derived along with Eq. (21). Hence, Eq. (22) is obtained.

$$\begin{aligned} \dot{V}_{do} &= e(\dot{\sigma} - \dot{R}_o) \\ &= e\cdot\frac{\sigma\cos\phi(\dot{x}_{cco} - \dot{x}_d) + \sigma\sin\phi(\dot{y}_{cco} - \dot{y}_d)}{\sigma} \\ &= e(-u_{do}\cos(\psi_{do} - \phi) - V_o) \end{aligned} \tag{22}$$

Furthermore, substituting (19) into (22), the derivative $\dot{V}_{do}$ yields as Eq. (23).

$$\dot{V}_{do} = \frac{-u_{do}e^2}{\sqrt{(e+\kappa)^2 + \iota^2 R_o^2}} \le -\frac{2u_{do}}{\sqrt{(R_m - R_o + \kappa)^2 + \iota^2 R_o^2}}V_{do} \tag{23}$$

According to the closed-loop gain shaping algorithm (Zhang, 2012), $V_{do}(t)$ is asymptotically stable, i.e., $\lim_{t\to\infty} V_{do}(t) = 0$. The error signal e would converge to 0 for $t \to \infty$. That is, the DVS would navigate to the boundary of the anti-collision space, which provides the obstacles avoidance guidance for the real ship. In addition, the validity of Eq. (16) can be obtained by following the similar analysis.

Remark 3. The above analysis focuses on the moving obstacle. And that can also be applied to the static one, which is a special case of a moving obstacle.

In this principle, the objective is to guide the real ship to track the waypoints-based reference path in presence of multiple static and moving obstacles. It is achieved by switching between the path-following mode and the obstacles avoidance one. During the switching process, to obtain the smooth orders for DVS, the transitional function (24) is employed.

$$\psi_d = \begin{cases} (1 - \varepsilon(t))\psi_{d1} + \varepsilon\psi_{d2}, & t_c \le t < t_c + t_s \\ \psi_{d2}, & t \ge t_c + t_s \end{cases} \tag{24}$$

where ψ_{d1}, ψ_{d2} are the DVS's heading orders for the previous mode and the current mode, respectively. $\varepsilon(t) = \sin(\pi(t - t_c)/t_s - \pi/2)/2 + 1/2$. t_c is the switching time point and t_s indicates the switching duration. In addition, the identical transition is applied to the speed order u_d of DVS.

4. Robust adaptive control with the finite-time performance

In this section, the finite-time control law is developed to guarantee the convergence of the real ship to the DVS. One quantifies the objective by defining the tracking error (25), whose derivative can be derived as Eq. (26). Thus, Eqs. (26) and (2) could describe the error dynamics between the real ship and the DVS.

$$\begin{bmatrix} x_e \\ y_e \\ \psi_e \end{bmatrix} = \begin{bmatrix} \cos(\psi) & \sin(\psi) & 0 \\ -\sin(\psi) & \cos(\psi) & 0 \\ 0 & 0 & 1 \end{bmatrix}\begin{bmatrix} x_d - x \\ y_d - y \\ \psi_d - \psi \end{bmatrix} \tag{25}$$

$$\begin{cases} \dot{x}_e = -u + u_d\cos(\psi_e) + ry_e \\ \dot{y}_e = -v + u_d\sin(\psi_e) - rx_e \\ \dot{\psi}_e = r_d - r \end{cases} \tag{26}$$

4.1. Control design

Step 1: To stabilize the kinematic error dynamics (26), one can directly choose α_u, α_{ψ_e} and α_r as the virtual controls of the intermediate variables u, ψ_e and r. The virtual control laws are designed as Eq. (27).

$$\begin{aligned} &\alpha_u = k_x x_e^p + u_d\cos\psi_e, \\ &\alpha_{\psi_e} = \arctan\left(\frac{-k_y y_e^p + v - u_d^2 y_e/4}{u_d^\star}\right), \\ &\alpha_r = -k_\psi\tilde{\psi}_e^p + r_d - \dot{\alpha}_{\psi_e} \end{aligned} \tag{27}$$

In (27), k_x, k_y, k_ψ are positive design parameters, $\tilde{\psi}_e = \alpha_{\psi_e} - \psi_e$ is an error variable. $p = p_1/p_2$, $0 < p_1 < p_2$ and p_1, p_2 are both odd numbers. For the term $u_d\sin(\psi_e)$ in Eq. (26), $u_d^\star$ is an auxiliary reference speed with the following form (28) to guarantee the stabilization of y_e. In the

marine practice, the attitude error between the real ship and the DVS is normally small. That is, the condition $u_d \geq |-k_y y_e^p + v - u_d^2 y_e/4|$ is often satisfied. For the very few extreme cases $u_d < |-k_y y_e^p + v - u_d^2 y_e/4|$, the assignment $u_d^\star = u_d$ is to accelerate the convergence of the sway motion. That confirms to the ship manoeuvring experience and is easy to understand in Fig. 1.

$$u_d^\star = \begin{cases} \sqrt{u_d^2 - (-k_y y_e^p + v - u_d^2 y_e/4)^2}, \\ \quad \text{if } u_d \geq |-k_y y_e^p + v - u_d^2 y_e/4| \\ u_d, \quad \text{if } u_d < |-k_y y_e^p + v - u_d^2 y_e/4| \end{cases} \tag{28}$$

Based on Eq. (27), one defines the new error variables $u_e = \alpha_u - u$, $r_e = \alpha_r - r$. And the further deduction requires the first-order derivative of the virtual controls. Considering their physical realizability in the engineering practice, the derivative could be obtained by employing a second-order filter. Take α_u as a example, the corresponding filter is given in Eq. (29). That is a common method to prevent the repeated differentiations of virtual controls in the existing literature and does not affect the stability of the closed-loop system (Fossen, 2011; Zhao et al., 2014).

$$H_u(s) = \frac{\alpha_{uf}}{\alpha_u} = \frac{\omega_u^2}{s^2 + 2\varsigma_u \omega_u s + \omega_u^2} \tag{29}$$

where the natural frequency ω_u and the damping ratio ς_u are two design parameters.

Step 2: In this step, one takes the time derivative of u_e and r_e along with (2), (27) and (29). The corresponding error dynamics (30) is obtained. It is noted that the control input $\tau_u = \frac{T_u}{m_u}|n|n$, $\tau_r = \frac{F_r}{m_r}\delta$.

$$\begin{aligned} \dot{u}_e &= \dot{\alpha}_u - f_u(\boldsymbol{v}) - \tau_u - d_{wu} \\ \dot{r}_e &= \dot{\alpha}_r - f_r(\boldsymbol{v}) - \tau_r - d_{wr} \end{aligned} \tag{30}$$

In (30), the nonlinear term $f_i(\boldsymbol{v})$ is the system uncertainty including unknown model parameters and structure, $i = u, r$. Based on the Lemma 5, it can be approximated by the RBF NNs.

$$\begin{aligned} -f_i(\boldsymbol{v}) &= \boldsymbol{S}(\boldsymbol{v})\boldsymbol{A}_i\boldsymbol{\alpha} - \boldsymbol{S}(\boldsymbol{v})\boldsymbol{A}_i\boldsymbol{v}_e + \varepsilon_i \\ &= \boldsymbol{S}(\boldsymbol{v})\boldsymbol{A}_i\boldsymbol{\alpha} - b_i\boldsymbol{S}(\boldsymbol{v})\boldsymbol{W}_i + \varepsilon_i \end{aligned} \tag{31}$$

where $\boldsymbol{\alpha} = [\alpha_u, v, \alpha_r]^{\mathrm{T}}$, $\boldsymbol{v}_e = [u_e, 0, r_e]^{\mathrm{T}}$, the approximating error ε_i has the unknown upper bound $\bar{\varepsilon}_i$. Defining $b_i = \|\boldsymbol{A}_i\|_{\mathrm{F}}$, $\boldsymbol{A}_i^m = \boldsymbol{A}_i/\|\boldsymbol{A}_i\|_{\mathrm{F}}$, then the expressions $\boldsymbol{W}_i = \boldsymbol{A}_i^m\boldsymbol{v}_e$ and $b_i\boldsymbol{W}_i = \boldsymbol{A}_i\boldsymbol{v}_e$ are obvious. Actually, the two NNs for $i = u, r$ are with the same basis function $\boldsymbol{S}(\boldsymbol{v})$ and the robust damping technique could effectively reduce the computing burden for weight updating (Zhang and Zhang, 2015). Thus, the design would require lower computational complexity when the proposed algorithm is implemented in the industrial processing unit.

Furthermore, the robust neural damping technique is applied and the error dynamics (30) is presented as Eq. (32). It is noted that the formula (33) is useful for constructing the robust damping term. In (33), $\vartheta_i = \max\{\|\boldsymbol{A}_i\|_{\mathrm{F}}, \bar{\varepsilon}_i + \bar{d}_{wi}\}$ is a unknown constant and the damping term $\varphi_i(\boldsymbol{v}) = \|\boldsymbol{S}(\boldsymbol{v})\|\|\boldsymbol{\alpha}\| + 1$.

$$\dot{i}_e = \dot{\alpha}_i - b_i\boldsymbol{S}(\boldsymbol{v})\boldsymbol{W}_i + (\boldsymbol{S}(\boldsymbol{v})\boldsymbol{A}_i\boldsymbol{\alpha} + \varepsilon_i - d_{wi}) - \tau_i \tag{32}$$

$$\begin{aligned} &\boldsymbol{S}(\boldsymbol{v})\boldsymbol{A}_i\boldsymbol{\alpha} + \varepsilon_i - d_{wi} \\ &\leq \|\boldsymbol{S}(\boldsymbol{v})\|\|\boldsymbol{A}_i\|_{\mathrm{F}}\|\boldsymbol{\alpha}\| + \bar{\varepsilon}_i + \bar{d}_{wi} \\ &\leq \vartheta_i\varphi_i(\boldsymbol{v}) \end{aligned} \tag{33}$$

In the proposed algorithm, one employs $\hat{\lambda}_u$, $\hat{\lambda}_r$ as estimations of $\lambda_u = \frac{m_u}{T_u}$, $\lambda_r = \frac{m_r}{F_r}$, which are updated online to compensate the system gain uncertainties. The estimation errors $\tilde{\lambda}_u = \hat{\lambda}_u - \lambda_u$, $\tilde{\lambda}_r = \hat{\lambda}_r - \lambda_r$. And the proposed scheme focuses on the measurable variables n and δ. The control law is presented in Eq. (34), where $\alpha_{\tau u}$, $\alpha_{\tau r}$ are two ideal intermediate variables for τ_u, τ_r. Moreover, the corresponding adaptive laws are given in Eq. (35), and the further synthesis analysis will be detailed in section 4.2.

$$\begin{aligned} &n = \mathrm{sgn}(N_2)\sqrt{|N_2|},\ N_2 = \hat{\lambda}_u\alpha_{\tau u}, \quad \delta = \hat{\lambda}_r\alpha_{\tau r} \\ &\alpha_{\tau u} = x_e + \dot{\alpha}_u + k_{u1}u_e^p + k_{u2}^{1+\frac{1}{p}}\Phi_u(\cdot)u_e^{\frac{1}{p}}, \\ &\alpha_{\tau r} = -\tilde{\psi}_e + \dot{\alpha}_r + k_{r1}r_e^p + k_{r2}^{1+\frac{1}{p}}\Phi_r(\cdot)r_e^{\frac{1}{p}} \end{aligned} \tag{34}$$

$$\dot{\hat{\lambda}}_i = \gamma_i[\alpha_{\tau i}i_e - \sigma_i(\hat{\lambda}_i - \hat{\lambda}_i(0))^p] \quad i = u, r \tag{35}$$

In Eqs. (34) and (35), $\Phi_i(\cdot) = \varphi_i^{1+\frac{1}{p}}(\cdot) + \|\boldsymbol{S}_i(\cdot)\|^{1+\frac{1}{p}}$, $i = u, r$. k_{i1}, k_{i2}, γ_i, σ_i, are all positive design parameters.

4.2. Stability analysis

Now, one states the main result of this note as follows.

Theorem 1. *For the error dynamic system (2) and (26) satisfying Assumption 1–3, the initial state conditions are within a compact set* Π, $\Pi := \{(x_e, y_e, \psi_e, u_e, v, r_e, \tilde{\lambda}_u, \tilde{\lambda}_r), x_e^2 + y_e^2 + \psi_e^2 + u_e^2 + v^2 + r_e^2 + \tilde{\lambda}_u^2 + \tilde{\lambda}_r^2 \leq 2\Delta\}$ *with any* $\Delta > 0$. *The control law (27), (34) and the adaptive law (35) will guarantee the semi-global practical finite-time bounded (SGPFB) property of the closed-loop system if the design parameters* k_x, k_y, k_ψ, k_{u1}, k_{u2}, k_{u3}, k_{r1}, k_{r2}, k_{r3}, γ_u, γ_r, σ_u, σ_r *are selected appropriately.*

Proof. *Choose the Lyapunov function candidate as* Eq. (36).

$$\begin{aligned} V = &\frac{1}{2}x_e^2 + \frac{1}{2}y_e^2 + \frac{1}{2}\tilde{\psi}_e^2 + \frac{1}{2}u_e^2 + \frac{1}{2}r_e^2 \\ &+ \frac{T_u}{2m_u\gamma_u}\tilde{\lambda}_u^2 + \frac{F_r}{2m_r\gamma_r}\tilde{\lambda}_r^2 \end{aligned} \tag{36}$$

The time derivative $\dot{V}$ *can be derived along* (26), (27) *and* (30), *i.e.* Eq. (37), *where* $\Psi_y = \sin\psi_e - \sin\alpha_{\psi_e}$. *In addition, according to the design in* Section 4.1, *the variables* τ_u, τ_r *can be expressed as* $\tau_u = \frac{T_u}{m_u}(\lambda_u + \tilde{\lambda}_u)\alpha_u$, $\tau_r = \frac{F_r}{m_r}(\lambda_r + \tilde{\lambda}_r)\alpha_r$.

$$\begin{aligned} \dot{V} = &-k_x x_e^{p+1} - k_y y_e^{p+1} - k_\psi\tilde{\psi}_e^{p+1} + u_e x_e - r_e\tilde{\psi}_e + \Psi_y^2 \\ &+ \textstyle\sum_{i=u,r}[\dot{\alpha}_i - b_i\boldsymbol{S}(\boldsymbol{v})\boldsymbol{W}_i + (\boldsymbol{S}(\boldsymbol{v})\boldsymbol{A}_i\boldsymbol{\alpha} + \varepsilon_i - d_{wi}) \\ &- \tau_i]i_e + \frac{T_u}{m_u\gamma_u}\tilde{\lambda}_u\dot{\hat{\lambda}}_u + \frac{F_r}{m_r\gamma_r}\tilde{\lambda}_r\dot{\hat{\lambda}}_r \end{aligned} \tag{37}$$

From Young's inequality and Lemmas 2-4, *the following* (38), (39) *and* (40) *would facilitate the further derivation*, $i = u, r$.

$$\begin{aligned} &(\boldsymbol{S}(\boldsymbol{v})\boldsymbol{A}_i\alpha + \varepsilon_i - d_{wi})i_e - b_i\boldsymbol{S}(\boldsymbol{v})\boldsymbol{W}_i i_e \\ &\leq k_{i2}^{1+\frac{1}{p}}\Phi_i(\cdot)i_e^{1+\frac{1}{p}} + \frac{b_i^{1+p}\|\boldsymbol{W}_i\|^{1+p}}{k_{i2}^{1+p}} + \frac{\vartheta_i^{1+p}}{k_{i2}^{1+p}} \end{aligned} \tag{38}$$

$$\|\boldsymbol{W}_i\|^{1+p} = \left(\frac{\|\boldsymbol{A}_i\boldsymbol{v}_e\|}{\|\boldsymbol{A}_i\|_{\mathrm{F}}}\right)^{1+p} \leq u_e^{1+p} + r_e^{1+p} \tag{39}$$

$$-\tilde{\lambda}_i(\hat{\lambda}_i - \hat{\lambda}_i(0))^p \leq -\frac{1-q}{1+p}\tilde{\lambda}_i^{p+1} + \frac{\ell_i}{1+p} \tag{40}$$

with

$$\ell_i = (\lambda_i - \hat{\lambda}_i(0))^{p+1} + \left[\frac{\lambda_i - \hat{\lambda}_i(0)}{1-(1-q)^{\frac{1}{1+p}}}\right] + \left[\frac{(\lambda_i - \hat{\lambda}_i(0))(1-q)^{\frac{1}{1+p}}}{1-(1-q)^{\frac{1}{1+p}}}\right]^{\frac{1}{1+p}}, \ i = u, r.$$

The parameters p, q *has been given in* Lemma 2.

Submitting the actual control law (34) *and* (35), *it is obtained as follows.*

$$\begin{aligned} \dot{V} = &-k_x x_e^{p+1} - k_y y_e^{p+1} - k_\psi\tilde{\psi}_e^{p+1} - \left(k_{u1} - \frac{b_u^{1+p}}{k_{u2}^{1+p}}\right. \\ &\left. - \frac{b_r^{1+p}}{k_{r2}^{1+p}}\right)u_e^{p+1} - \left(k_{r1} - \frac{b_u^{1+p}}{k_{u2}^{1+p}} - \frac{b_r^{1+p}}{k_{r2}^{1+p}}\right)r_e^{p+1} \\ &- \frac{(1-q)T_u\sigma_u}{(1+p)m_u}\tilde{\lambda}_u^{p+1} - \frac{(1-q)F_r\sigma_r}{(1+p)m_r}\tilde{\lambda}_r^{p+1} + \varrho \end{aligned} \tag{41}$$

where $\varrho = \|\Psi_y\|_\infty^2 + \frac{\vartheta_u^{1+p}}{k_{u2}^{1+p}} + \frac{\vartheta_r^{1+p}}{k_{r2}^{1+p}} + \frac{\ell_u\bar{T}_u\sigma_u}{(1+p)m_u} + \frac{\ell_r\bar{F}_r\sigma_r}{(1+p)m_r}$, *and* $\|\Psi_y\|_\infty := \sup_{t\geq 0}|\Psi_y(t)|$.

For the further tuning process, one defines the positive constant

$$c_1 = \min\left\{2^{\frac{1+p}{2}}k_x,\ 2^{\frac{1+p}{2}}k_y,\ 2^{\frac{1+p}{2}}k_\psi,\ \frac{(1-q)\sigma_u(2\gamma_u)^{\frac{1+p}{2}}T_{u0}^{\frac{1-p}{2}}}{(1+p)m_u^{\frac{1-p}{2}}},\ \frac{(1-q)\sigma_r(2\gamma_r)^{\frac{1+p}{2}}F_{r0}^{\frac{1-p}{2}}}{(1+p)m_r^{\frac{1-p}{2}}}\right\}$$

and selects the design parameters k_{u1}, k_{u2}, k_{r1}, k_{r2} *satisfying*

$$k_{u1} \geq 2^{-\frac{1+p}{2}}c_1 + \frac{b_u^{1+p}}{k_{u2}^{1+p}} + \frac{b_r^{1+p}}{k_{r2}^{1+p}},$$
$$k_{r1} \geq 2^{-\frac{1+p}{2}}c_1 + \frac{b_u^{1+p}}{k_{u2}^{1+p}} + \frac{b_r^{1+p}}{k_{r2}^{1+p}}.$$

Applying Lemma 4, Eq. (41) *can be further derived as* (42).

$$\dot{V} \leq -c_1 V^{\frac{1+p}{2}} + \varrho \tag{42}$$

Furthermore, according to the definition of V *and* Lemma 1, *the trajectories of the closed-loop system would converge into a small set containing the origin point in finite time. That implies that the immediate error variables* x_e, y_e, $\tilde{\psi}_e$, u_e, r_e, $\tilde{\lambda}_u$, $\tilde{\lambda}_r$ *would fall into and remain in the attractive set* Ω_b: $=\{(x_e, y_e, \tilde{\psi}_e, u_e, r_e, \tilde{\lambda}_u, \tilde{\lambda}_r)|x_e^{p+1} + y_e^{p+1} + \tilde{\psi}_e^{p+1} + u_e^{p+1} + r_e^{p+1} \leq 2^{\frac{1+p}{2}}B_0,\ \tilde{\lambda}_u^{p+1} \leq (2m_u\gamma_u/T_{u0})^{\frac{1+p}{2}}B_0,\ \tilde{\lambda}_r^{p+1} \leq (2m_r\gamma_r/F_{r0})^{\frac{1+p}{2}}B_0\}$ *with* $t \to T_R$, *see* Eq. (43), $B_0 = \frac{\varrho}{(1-q)c_1}$ *is a positive constant. And the bounded variable* B_0 *could be small enough by adjusting the design parameters appropriately. For some cases,* ϱ *may be lower bounded by the model parameters and cannot be made arbitrarily small. Though, to guarantee that the* B_0 *is small, the parameter* c_1 *can be tuned to be large enough by making the following control gains large:* k_x, k_y, k_ψ, k_{u1}, k_{u2}, k_{r1}, k_{r2}, γ_u, γ_r. *Considering the control law and adaptive law, all the state variables are bounded within the finite time, as well as the other immediate variables. Thus, the closed-loop control system is SGPFB stable under the proposed scheme.*

$$T_R = \frac{2}{(1-p)qc_1}\left[V^{\frac{1-p}{2}}(0) - \left(\frac{\varrho}{(1-q)c_1}\right)^{\frac{1-p}{1+p}}\right] \tag{43}$$

5. Illustrative experiments

In this section, two experiments are presented to illustrate the effectiveness of the proposed scheme, including the comparative experiment with the result in (Moe and Pettersen, 2016) and the experiment in the simulated ocean environment. For this purpose, the scientific research vessel YUKUN (length of 105m, displacement volume of 5710.2m^3) of Dalian Maritime University is selected as the plant that is equipped with the main propeller (Max. shaft velocity of 150rpm) and the steering rudder (Max. rudder angle of 30deg., Max. rudder rate of 2.8deg. /s). The model parameters are identified from the full-scale trial data and the actuated servo dynamics is considered in the model. The studies about the mathematical model has been published in the existing literature (Zhang et al., 2015; Zhang and Zhang, 2015).

5.1. Comparative experiment

The comparative experiment aims at verifying the effectiveness of the proposed DVS guidance principle, and its superiority in comparison of the existing result. In (Moe and Pettersen, 2016), the set-based LOS guidance is developed to achieve the path-following control of underactuated ships, with the function of single obstacle avoidance. While, in this note, the novel DVS principle is applicable for more sophisticated scenarios, including situations of the multi-static obstacles, the multi-moving obstacles and the multiple static/moving obstacles. Table 1 summarizes the comparison for applicability of the two principles.

Table 1
Comparison for applicability of the proposed guidance and the result in (Moe and Pettersen, 2016).

Scenarios	Applicability (Yes/No)	
	The proposed guidance	The compared result
Abiding COLREGs	Yes	Yes
Single static obstacle	Yes	Yes
Single moving obstacle	Yes	Yes
Multi-static obstacles	Yes	No
Multi-moving obstacles	Yes	No
Multiple static/moving obstacles	Yes	No
Avoidance guidance on the straight-line stage	Yes	Yes
Avoidance guidance on the curve stage	Yes	No
Speed regulation	Yes	No

As for the guidance performance, one only consider the head-on scenario without considering the external disturbance. The reference path is generated by waypoints W_1(200m, 0m), W_2(200m, 800m). The moving obstacle is set as a ship with length of 85m, the surge speed of 4.1m/s. The initial state for the real ship and the obstacle ship are $[x(0), y(0), \psi(0), u(0), v(0), r(0)]_{\text{Real ship}}$ = [0m, 0m, 85deg, 4.9m/s, 0.2m/s, 0deg/s], $[x(0), y(0), \psi(0), u(0), v(0), r(0)]_{\text{Obstacle}}$ = [180m, 800m, 270 deg,4.1m/s, 0.0m/s, 0deg/s], respectively. For the proposed guidance law, one set parameters for the detectable space and the anti-collision space, R_m = 180m, R_o = 75m. The convergence coefficient ι = 0.85. For the DVS, the desired path-following speed and the avoidance one u_{do} = 6.0m/s. Whereas, for the compared result, the parameter setting refers to the result in (Moe and Pettersen, 2016). Moreover, one need to tune the looking-ahead distance Δ= 75m because of that the manoeuvrability of YUKUN is different from that of the plant in (Moe and Pettersen, 2016).

Fig. 4 and Fig. 5 illustrate the avoidance manoeuvring in the head-on situation. The detectable space and the anti-collision space are denoted by circles of the dotted line. From the comparison, both of two principles could provide the effective guidance to implement the avoidance manoeuvring, and abided by the COLREGs. Though, the superiority of the DVS-based guidance is obvious. E.g., the proposed guidance would regulate the surge speed during the avoidance process. That can diminish the impact of speed loss, which is a prevalent characteristic of the large-scale ship. In Fig. 5, the desired yaw angle (i.e. the yaw angle of DVS) is more reasonable under the proposed guidance law. While, the compared scheme is with evident chartering dynamics. That verify that the proposed principle is more consistent with the marine practice.

5.2. Experiment in the simulated ocean environment

In this section, in order to illustrate the robustness and effectiveness of the proposed scheme, it is implemented a waypoints-based path-following experiment in presence of the multiple static and moving obstacles and the simulated ocean disturbances. For this purpose, the physical based mathematical models (Fossen, 2011) are employed for the sea wind and the irregular wind-generated waves. Fig. 6 gives the detailed block diagram for the simulation experiment, where the marked numbers denote formulas involved in the relative block. In the experiment, the wind direction is set as ψ_{wind} = 200deg, the average velocity V_{wind} = 15.7m/s. By virtue of the JONSWAP spectrums, the wind-generated wave forces/moments are simulated, which corresponds to the sixth level sea state. The corresponding graphs of the simulated wind and waves are shown in Fig. 7.

The waypoints-based reference path is defined by waypoints W_1(200m, 0m), W_2(200m, 1000m), W_3(1200m, 1500m), W_4(1200m, 2500m).

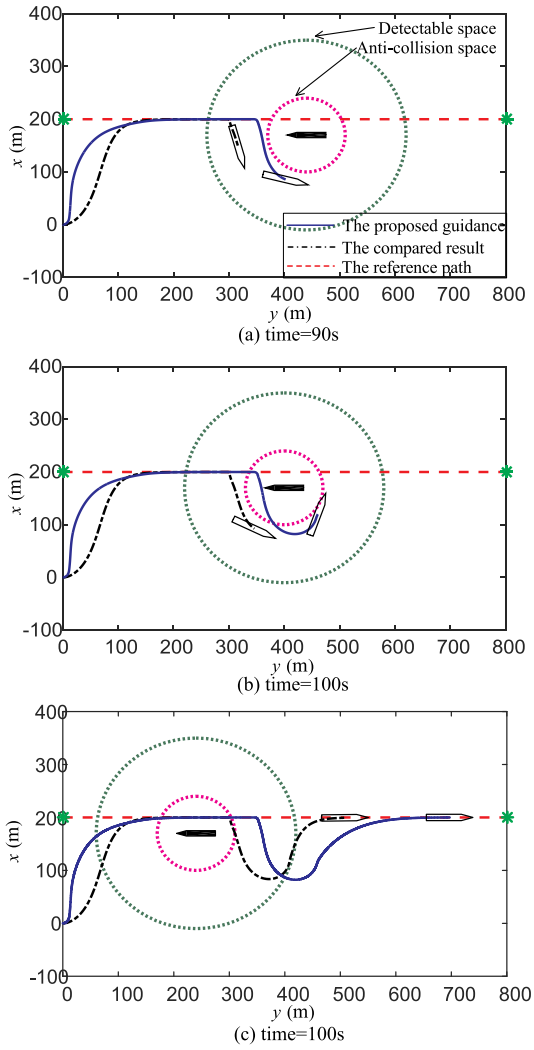

Fig. 4. Comparison of the avoidance trajectory: the proposed guidance and the result in (Moe and Pettersen, 2016).

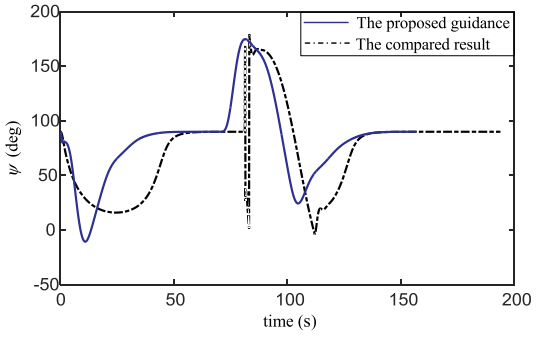

Fig. 5. Comparison of the desired yaw angle: the proposed guidance and the result in (Moe and Pettersen, 2016).

The static obstacles are set with the anti-collision space of different size and distribute around the reference path. While, the moving obstacles are with the different speed and starting time. To simplify the simulation test, one selects the same size for the moving obstacles' anti-collision space and detectable one, i.e., $R_o = 75$m and $R_m = 187$m. The initial states for the real ship is same to that of Section 5.1. The detailed parameter setting for the DVS-based guidance and the robust neural control law is given in Table 2.

Remark 4. *In the experiment, the related parameters are tuned by using the trial and error strategy. As for the control parameters, it is known that the gain parameters should be large enough to ensure the control performance and another consideration is that the large parameter setting would lead to unexpected large control signals. Therefore, in general, one first sets large value for the gain parameters,* e.g. $k_x, k_y, \cdots, \gamma_r$. *Then, the parameters should be reduced properly by testing the simulation runs. That could guarantee that the parameter setting is effective in the practical engineering. Following the similar procedure, the number of NNs node should be smallest and can ensure the capability to approximate the model uncertainty sufficiently. Finally, the RBF NN* $\boldsymbol{S}(\boldsymbol{v})\boldsymbol{A}_i\boldsymbol{v}$ *contain 21 nodes in the control law (34), with centers spaced in* $[-5\text{m/s}, 15\text{m/s}]$ *for the surge speed u,* $[-5\text{m/s}, 5\text{m/s}]$ *for the sway speed v and* $[-0.6\text{rad/s}, 0.6\text{rad/s}]$ *for the yaw velocity r, widths* $\xi_i = 3\,(i = 1,2,\cdots,l)$.

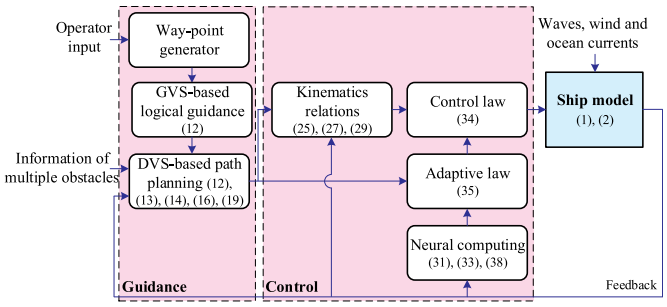

Fig. 6. The detailed block diagram for the simulation experiment.

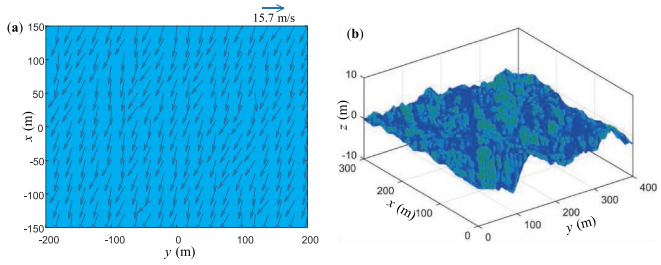

Fig. 7. The simulated environmental disturbances with the sixth level sea state: (a) the sea wind, (b) the irregular waves.

Fig. 8, Fig. 9 and Fig. 10 present simulation results of the experiment. To verify the effectiveness of the proposed scheme clearly, it includes four subfigures corresponding to four time points, i.e. time = 240s, 290s, 345s, 600s. In Fig. 8(a), the own ship has passed the first section of the reference path, where there exist concentrated static obstacles. And the DVS-based law could provide the effective guidance to implement the avoidance manoeuvering. For example, at time = 240s, the real ship encounters a dangerous crossing situation, where the obstacle ship is on the port side. Since it is not considered in this note that the moving obstacle could voluntarily avoid the real ship, the real ship turns to starboard to avoid the obstacle ship. At time = 290s, another crossing situation is encountered, and the real ship avoid the obstacle ship from the astern of her. That is in accordance with the COLREGs rule "When two power-driven ships are crossing, the ship which has the other on the starboard side must give way and avoid

Table 2
Detailed parameter setting for the proposed scheme.

Indexes	Parameters
Guidance part	$u_g = u_{dp} = 5.0$m/s, $u_{do} = 6.0$m/s, $l_{dbset} = 200$m.
	$k_d = 0.05$, $\iota = 0.45$, $\zeta = 0.52$, $t_s = 2$s.
Control part	$k_x = 1.8$, $k_y = 2.1$, $k_\psi = 0.8$, $p = 3/5$.
	$k_{u1} = 2.0 \times 10^5$, $k_{u2} = 2.5$, $k_{r1} = 1.3$, $k_{r2} = 2.0$.
	$\gamma_u = 0.15$, $\gamma_r = 0.20$, $\sigma_u = 0.50$, $\sigma_r = 0.35$.

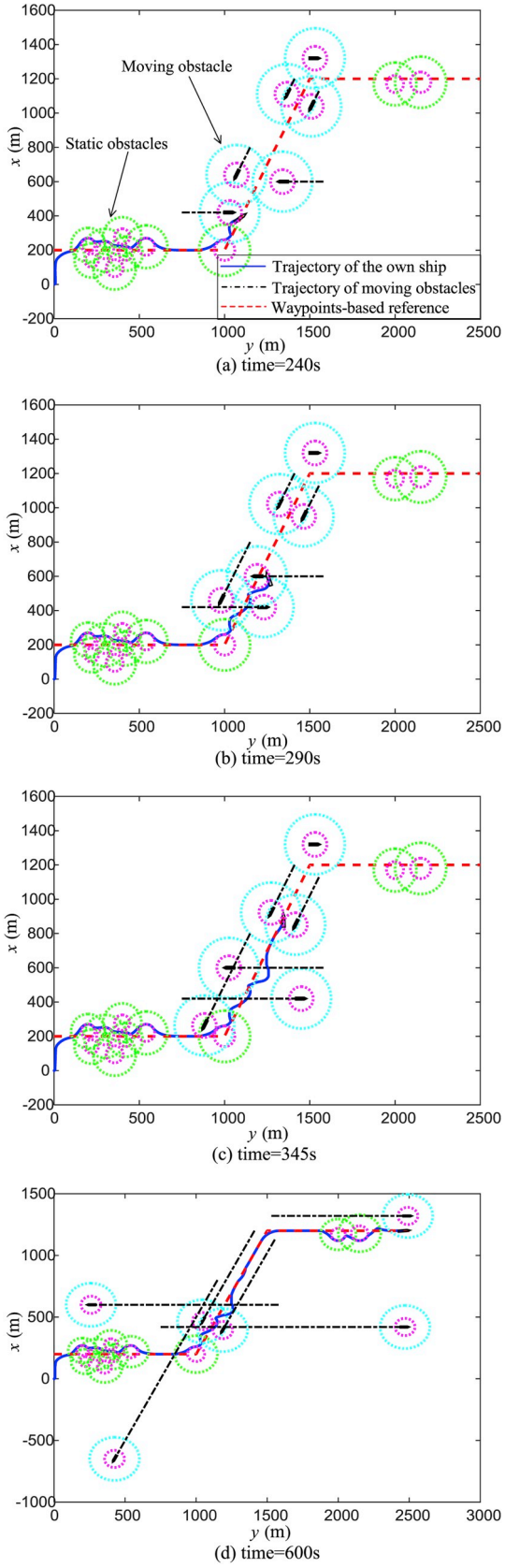

Fig. 8. The path-following trajectory for the experiment in presence of multiple static and moving obstacles: (a) time = 240s, (b) time = 290s, (c) time = 345s, (d) time = 600s.

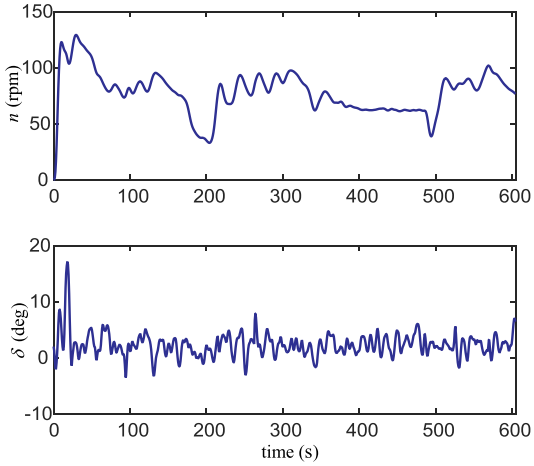

Fig. 9. Control inputs n, δ for the experiment in presence of multiple static and moving obstacles.

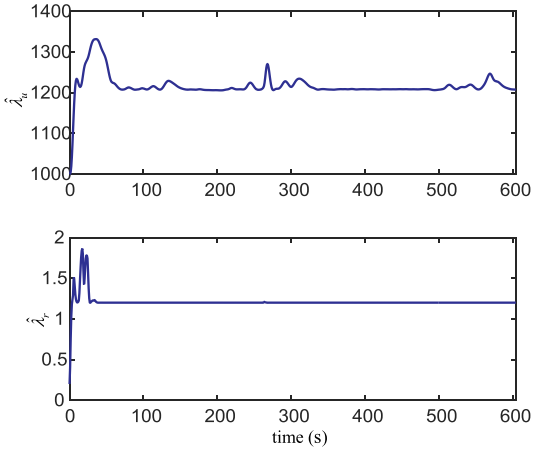

Fig. 10. Adaptive parameters $\hat{\lambda}_u$, $\hat{\lambda}_r$ for the experiment in presence of multiple static and moving obstacles.

crossing ahead of her". Fig. 8(b) and (c) verify the avoidance capability of the scheme to the multi-moving obstacles. After past and clear, the real ship could rapidly converge back to the path-following mode and be stabilized to the reference path. Meanwhile, the operation process is in accordance to the recommendation in the COLREGs. Fig. 8(d) is to show the overall trajectory of the experiment. Based on the above analysis, the proposed scheme is with robustness to the external disturbances, and could accomplish the path-following mission with the multiple obstacles avoidance function.

Figs. 9 and 10 present control efforts and the estimation of adaptive parameters. For merits of the DVS-based guidance, the control inputs are all within the reasonable range, i.e. [0rpm, 150rpm] for the shaft speed n and [−35deg, 35deg] for the rudder angle δ. Thus, it has been verified that the proposed scheme is with the good performance in the nautical practice.

6. Conclusion

In this note, an unified strategy is studied for the waypoints-based path-following control for underactuated ships in presence of multiple static and moving obstacles. A systematic DVS-based guidance principle is developed to improve the autonomy of marine ships, including the

path-following mode and the obstacles avoidance one. The priority selecting strategy can guarantee the smooth and flexible switch. Furthermore, a robust neural control algorithm is proposed to stabilize attitudes of the real ship to converge to that of DVS in finite time. And the SGPFB stability of the closed-loop system is proved by employing the Lyapunov theory. Different from the existing results, the performance of the proposed scheme is with higher intelligent level, being capable to avoid multi-static and multi-moving obstacles automatically and requiring no information about the system model and the external disturbance. The experiments are implemented under the simulated ocean environment and the results have illustrated the effectiveness of the proposed scheme.

Acknowledgement

This research is partially supported by the National Postdoctoral Program for Innovative Talents (No. BX201600103), the Doctoral Scientific Research Foundation of Liaoning Province (No.20170520189, 20180520039), the Program for Innovative Research Team in University (No.IRT17R13), the Fundamental Research Funds for the Central Universities(No.3132018301, 3132018304, 3132016315), the National Natural Science Foundation of China (No.61473183,51679024) and the China Postdoctoral Science Foundation (No.2016M601600). The authors would like to thank anonymous reviewers for their valuable comments to improve the quality of this article.

Appendix A. Proof of Lemma 2

Proof. In this part, one assumes the condition $a \geq 0$ and the proof for $a < 0$ could be done following the same flow.

By employing the homogeneous system theory (Tang et al., 2016; Li and Wang, 2013), Eq. (A.1) can be obtained.

$$\begin{aligned} &-x(x+a)^p = a(x+a)^p - (x+a)^{p+1} \\ &\leq -\frac{1}{1+p}x^{1+p} + \frac{1}{1+p}a^{1+p} + \underbrace{\frac{1}{1+p}[x^{1+p} - (x+a)^{1+p}]}_{\mathrm{F}} \end{aligned} \tag{A.1}$$

For $x \geq -a/2$, it is obvious that $\mathrm{F} \leq 0$. Thus, one can get Eq. (A.2) from Eq. (A.1).

$$-x(x+a)^p = -\frac{1}{1+p}x^{1+p} + \frac{1}{1+p}a^{1+p} \tag{A.2}$$

For $x < -a/2$, one try to find the necessary and sufficient condition for $\mathrm{F} \leq (q/(1+p))x^{1+p}$, i.e. satisfying Eq. (A.3). Then the inequality could be presented as (A.4).

$$(x+a)^{1+p} \geq (1-q)^{1+p} \tag{A.3}$$

$$-x(x+a)^p \leq -\frac{1-q}{1+p}x^{1+p} + \frac{1}{1+p}a^{1+p} \tag{A.4}$$

To obtain the necessary and sufficient condition for (A.3), the discussions includes two terms: (1) If $-a \leq x < -a/2$, one can obtain $x \geq -a/(1+(1-q)^{1/(1+p)})$ from Eq. (A.3). (2) For $x < -a$, $x \leq -a/(1-(1-q)^{1/(1+p)})$. Based on the above analysis, the necessary and sufficient condition can be derived as $x \leq -a/(1-(1-q)^{1/(1+p)})$ and $-a/(1+(1-q)^{1/(1+p)}) \leq x < -a/2$.

For the residual interval $-a/(1-(1-q)^{1/(1+p)}) < x < -a/(1+(1-q)^{1/(1+p)})$, F is monotonically decreasing. One can obtain the maximum of Eq. (A.1) at the index point $x = -a/(1-(1-q)^{1/(1+p)})$. Therefore, the inequality (6) holds. The Proof of Lemma 2 is completed.

References

Bertram, V., 2012. Practical Ship Hydrodynamics: Convention on the International Regulations for Preventing Collisions at Sea (COLREGs, 1972). The International Maritime Organisation (IMO).
Caharija, W., Pettersen, K., Bibuli, M., 2014. Integral line-of-sight guidance and control of underactuated marine vehicles: theory, simulations, and experiments. IEEE Trans. Contr. Syst. Technol. 24, 1623–1642.
Campbell, S., Naeem, W., Irwin, G., 2012. A review on improving the autonomy of unmmaned surface vehicles through intelligent collision avoidance manoeuvres. Annu. Rev. Contr. 36, 267–283.
Chen, M., Ge, S.S., Choo, Y.S., 2009. Neural network tracking control of ocean surface vessels with input saturation. In: Proceedings of the IEEE International Coference on Automation and Logistics, Shenyang,China, pp. 85–89.
Do, K.D., 2010. Practical control of underactuated ships. Ocean Eng. 37, 1111–1119.
Do, K.D., Pan, J., 2006. Global robust adaptive path following of underactuated ships. Automatica 42, 1713–1722.
Fossen, T., Pettersen, K., 2014. On uniform semiglobal exponential stability (usges) of proportional line-of-sight guidance laws. Automatica 50, 2912–2917.
Fossen, T.I., 2011. Handbook of Marine Craft Hydrodynamics and Motion Control. Wiley, New York.
Ghommam, J., Mnif, F., Derbel, N., 2010. Global stabilisation and tracking control of underactuated surface vessels. IET Control Theory & Appl. 4, 71–88.
Godhavn, J.M., Fossen, T.I., Berge, S.P., 1998. Nonlinear and adaptive backstepping designs for tracking control of ships. Int. J. Adapt. Contr. Signal Process. 12, 649–668.
Huang, J., Wen, C., Song, W.W.Y.D., 2016. Design of adaptive finite-time controllers for nonlinear uncertain systems based on given transient specifications. Automatica 69, 395–404.
Khatib, O., 1986. Real-time obstacle avoidance for robot manipulator and mobil robots. Int. J. Robot Res. 5, 90–98.
Kozynchenko, A.I., Kozynchenko, S.A., 2018. Applying the dynamic predictive guidance to ship collision avoidance: crossing case study simulation. Ocean Eng. 164, 640–649.
Kuwata, Y., Wolf, M.T., Zarzhitsky, D., Huntsberger, T.L., 2014. Safe maritime autonomous navigation with colregs using velocity obstacles. IEEE J. Ocean. Eng. 39, 110–119.
Li, J.H., Lee, P.M., Jun, B.H., Lim, Y.K., 2008. Point-to-point navigation of underactuated ships. Automatica 44, 3201–3205.
Li, S., Wang, X., 2013. Finite time consensus and collisioin avoidance control algorithms for multiple AUVs. Automatica 49, 3359–3367.
Li, T.S., Wang, D., Feng, G., Tong, S.C., 2010. A DSC approach to robust adaptive NN tracking control for strict-feedback nonlinear systems. IEEE Trans. Syst. Man Cybern. B Cybern. 40, 915–927.
Li, Y., Sui, S., Tong, S., 2017. Adaptive fuzzy control design for stochastic nonlinear switched systems with arbitrary switchings and unmodeled dynamics. IEEE Trans. Cybern. 47, 403–414.
Li, Y., Tong, S., Li, T., 2015. Composite adaptive fuzzy output feedback control design for uncertain nonlinear strict-feedback systems with input saturation. IEEE Trans. Cybern. 45, 2299–2308.
Lin, X., Nie, J., Jiao, Y., Liang, K., Li, H., 2018. Adaptive fuzzy output feedback stabilization control for the underactuated surface vessel. Appl. Ocean Res. 74, 40–48.
Liu, L., Wang, D., Peng, Z., Wang, H., 2016. Predictor-based los guidance law for path following of underactuated marine surface vehicles with sideslip compensation. Ocean Eng. 124, 340–348.
Liu, Y., Bucknall, R., 2015. Path planning algorithm for unmanned surface vehicle formations in a practical maritime environment. Ocean Eng. 97, 126–144.
Moe, S., Pettersen, K.Y., 2016. Set-based line-of-sight (los) path following with collision avoidance for underactuated unmanned surface vessel. In: Mediterranean Conference on Control and Automation, Athens,Greece.
Naeem, W., Irwin, G., Yang, A., 2012. COLREGs-based collision avoidance strategies for unmmaned surface vehicles. Mechatronics 22, 669–678.
Park, B.S., 2017. A simple output-feedback control for trajectory tracking of underactuated surface vessels. Ocean Eng. 143, 133–139.
Rodríguez-Seda, E., Tang, C., Spong, M., Stipanović, D., 2014. Trajectory tracking with collision avoidance for nonholonomic vehicles with acceleration constraints and limited sensing. Int. J. Robot Res. 33, 1569–1592.
Shojaei, K., 2016. Observer-based neural adaptive formation control of autonomous surface vessels with limited torque. Robot. Autonom. Syst. 78, 83–96.
Soltan, R.A., Ashrafiuon, H., Muske, K.R., 2011. Ode-based obstacle avoidance and trajectory planning for unmanned surface vessels. Robotica 29, 691–703.

Tae Hwan Lee, H.C., Myung, H., 2011. Multi-resolution path planning for marine surface vehicle considering environmental effects. In: IEEE-oceans, Spain, pp. 1–9.
Tam, C., Bucknall, R., Greig, A., 2009. Review of collision avoidance and path planning methods for ships in close range encounters. J. Navig. 62, 455–476.
Tang, Z.L., Ge, S.S., Tee, K.P., He, W., 2016. Robust adaptive neural tracking control for a class of perturbed uncertain nonlinear systems with state constraints. IEEE Trans. Syst. Man Cybern.: Systems 46, 1618–1629.
Wang, N., Qian, C., Sun, J., Liu, Y., 2016. Adaptive robust finte-time trajectory tracking control of fully actuated marine surface vehicles. IEEE Trans. Contr. Syst. Technol. 24, 1454–1462.
Yu, C., Xiang, X., Lapierre, L., Zhang, Q., 2017. Nonlinear guidance and fuzzy control for three-dimensional path following of an underactuated autonomous underwater vehicle. Ocean Eng. 146, 457–467.
Zereik, E., Sorbara, A., Bibuli, M., 2015. Priority task approach for usvs' path following missions with obstacle avoidance and speed regulation. In: Ifac Conference on Manouvering and Control of Marine Craft, pp. 25–30.
Zhang, G., Cai, Y., Zhang, W., 2017a. Robust neural control for dynamic positioning ships with the optimum-seeking guidance. IEEE Trans. Syst. Man Cybern.: Systems 47, 1500–1509.
Zhang, G., Zhang, X., 2014. Concise robust adaptive path-following control of underactuated ships using dsc and mlp. IEEE J. Ocean. Eng. 39, 685–694.
Zhang, G., Zhang, X., 2015. A novel DVS guidance principle and robust adaptive path-following control for underactuated ships using low frequency gain-learning. ISA (Instrum. Soc. Am.) Trans. 56, 75–85.
Zhang, G., Zhang, X., 2016. Practical robust neural path following control for underactuated marine vessels with actuators uncertainties. Asian J. Contr. 19, 173–187.
Zhang, G., Zhang, X., Pang, H., 2015. Multi-innovation auto-constructed least squares identification for 4 DOF ship manoeuvring modelling with full-scale trial data. ISA (Instrum. Soc. Am.) Trans. 58, 186–195.
Zhang, J., Sun, T., Liu, Z., 2017b. Robust model predictive control for path-following of underactuated surface vessels with roll constraints. Ocean Eng. 143, 125–132.
Zhang, W., 2012. Quantitative Process Control Theory. CRC Press, New York.
Zhao, Z., He, W., Ge, S., 2014. Adaptive neural network control of a fully actuated marine surface vessel with multiple output constraints. IEEE Trans. Contr. Syst. Technol. 22, 1536–1543.
Zou, A., Kumar, K.D., Hou, Z., Liu, X., 2011. Finite-time attitude tracking control for spacecraft using terminal sliding mode and Chebyshev neural network. IEEE Trans. Syst. Man Cybern.: Systems 44, 950–963.